DOI: 10.6060/mhc245905k

Oxygen Activation Process *vs* the Metal-Organic Frameworks Structure

Vyacheslav A. Kulev,[@] Igor V. Novikov, Nadezhda M. Berezina, Mikhail I. Bazanov, and Tatyana A. Ageeva

Ivanovo State University of Chemistry and Technology, 153000 Ivanovo, Russian Federation
[@]Corresponding author E-mail: slava.kulev@mail.ru

Dedicated to the memory of Academician of Russian Academy of Sciences Oskar I. Koifman

Cobalt tetra- ($CoPc(COOH)_4$) and octacarboxyphthalocyanines ($CoPc(COOH)_8$) were obtained as starting blocks for the formation of metal-organic framework (MOFs). On their basis the corresponding MOFs containing aluminum oxide clusters of various structures as a binding component were synthesized. The activity of these materials as heterogeneous catalysts for the oxidation of 4-tert-butylpyrocatechol with atmospheric oxygen was studied. It was found that MOF based on octacarboxy cobalt phthalocyanine ($CoPc(COO)_8H_4Al_2$) has greater activity compared to MOF based on tetracarboxy cobalt phthalocyanine ($CoPc(COO)_4Al$). At the same time, the rate of the oxidation reaction of 4-tert-butylpyrocatechol catalyzed by $CoPc(COO)_8H_4Al_2$ is 5.5 times higher than for $CoPc(COO)_4Al$ under equal conditions. The study of the electroreduction of molecular oxygen on graphite electrodes modified with both the cobalt phthalocyanines and MOF obtained on their basis was carried out to confirm the catalytic activity of the materials under study in the process of oxygen activation. It has been shown that $CoPc(COOH)_4$ exhibits greater activity compared to $CoPc(COOH)_8$ in the oxygen electroreduction processes. The resulting disagreements most likely indicate a large contribution of the MOFs structure to the catalysis processes. The morphology of the obtained materials was assessed using electron scanning microscopy. The structures of the studied compounds were optimized using quantum chemical modeling methods. Combination of the literature and obtained data made it possible to show the structures of synthesized MOFs for the first times, which are indirectly confirmed by experimental data.

Keywords: Phthalocyanine, metal-organic frameworks, catalyst, oxygen electroreduction, quantum-chemical calculation.

Влияние структуры металлоорганических каркасных соединений на процесс активации кислорода

В. А. Кулёв,[@] И. В. Новиков, Н. М. Березина, М. И. Базанов, Т. А. Агеева

Ивановский государственный химико-технологический университет, 153000 Иваново, Россия
[@]E-mail: slava.kulev@mail.ru

Посвящается памяти Академика РАН Оскара Иосифовича Койфмана

Получены тетра- ($CoPc(COOH)_4$) и октакарбоксифталоцианинаты кобальта ($CoPc(COOH)_8$) как исходные блоки для формирования металлорганических каркасных структур (МОКС). На основе полученных фталоцианинатов синтезированы соответствующие МОКС, в которых в качестве связующего компонента выступают алюмооксидные кластеры различной структуры. Изучена активность данных материалов в качестве гетерогенных катализаторов реакции окисления 4-трет-бутилпирокатехина кислородом воздуха. При исследовании каталитического процесса обнаружено, что МОКС на основе октакарбоксифталоцианината кобальта ($CoPc(COO)_8H_4Al_2$) обладает большей активностью по сравнению с МОКС на основе тетракарбоксифталоцианината ($CoPc(COO)_4Al$). При этом скорость реакции окисления 4-трет-бутилпирокатехина, катализируемой $CoPc(COO)_8H_4Al_2$, в 5,5 раз больше, чем для $CoPc(COO)_4Al$ при одинаковых условиях. Для подтверждения каталитической активности исследуемых материалов в процессе активации кислорода проведено исследование электровосстановления молекулярного кислорода на графитовых

электродах, модифицированных как исходными фталоцианинатами кобальта, так и полученными на их основе МОКС. Показано, что $CoPc(COOH)_4$ проявляет большую активность по сравнению с $CoPc(COOH)_8$ в реакции электровосстановления молекулярного кислорода. Полученные разногласия вероятнее всего свидетельствуют о большом вкладе структуры исследуемых МОКС в процессы катализа. Морфология полученных материалов оценена с использованием метода электронной сканирующей микроскопии. Методами квантовохимического моделирования оптимизированы структуры исследованных соединений. Обобщение литературных и полученных данных позволило впервые показать структуры синтезированных МОКС, которые косвенно подтверждаются экспериментальными данными.

Ключевые слова: Фталоцианины, металлоорганические каркасные соединения, катализ, электровосстановление кислорода, квантово-химическое моделирование.

Introduction

Today, a huge number of energy carriers and materials have been developed to improve comfort, health and safety. Catalysis has made it possible to produce polymers, pharmaceuticals, synthetic fertilizers, detergents and much more.

In addition, catalysis is also used to purify air and water from various environmentally harmful pollutants.[1] In the production processes of more than 90% of all chemical products, at least one catalytic stage is present.[2] At the same time, heterogeneous catalysis was historically the first to receive widespread industrial use and is still used in three-quarters of all catalytic processes in industry.[3]

Scientists of the 21st century have significantly increased interest in the study of catalytic processes. Several catalytic methods have received the greatest development, for example, transition metal catalysis, organocatalysis, photocatalysis, electrocatalysis and biocatalysis.[4,5] The most popular are metal-based catalysts, which are widely used in the synthesis of new organic compounds. They can be in the form of porous metal materials, metal salts, metal oxides, or metal complexes with organic and inorganic ligands. Such compounds can be used as catalysts under homogeneous, heterogeneous conditions, or onto solid support conditions.[6,7]

Today, metal complex catalysts are a very promising area of research. In such catalysts, metal ions are surrounded by organic ligands, allowing all atoms to exhibit catalytic activity. In addition, by changing the nature and structure of the ligand, it is possible to achieve the necessary activity and also stereo-selectivity of the catalyzed process.[3] Basically, metal complex catalysis is carried out under homogeneous conditions,[8-11] which causes some difficulties in separating the catalyst and purifying the target product. On the contrary, catalysts obtained on polymer supports can be more easily separated from the reaction mass. But methods of binding a metal ion to a support are usually of a coordination or chelate nature,[12,13] and as a result, metal atoms tend to be washed out of the polymer support and contaminate the target product.

The problem of loss of essential metals and contamination of the product with them can be solved by using tetrapyrrole macroheterocyclic compounds as ligands.[14-16] These compounds can coordinate most metal cations[17] and tough hold them in the central coordination cavity. One of the promising and available macroheterocycles are phthalocyanines. The synthesis of phthalocyanines is carried out in one pot and can achieve quantitative yields.

Tetra- and octacarboxy substituted phthalocyanines are quite interesting, since the precursors for their synthesis are cheap, accessible and produced on an industrial scale. In addition, the synthesis and purification of these phthalocyanines is low-cost and does not require specific waste disposal, since only aqueous solutions of acids and alkalis are used. At the moment, there is an active study of the catalytic properties of carboxy substituted phthalocyanines as part of covalent organic frameworks (COF) in oxygen reduction reaction,[18,19] CO_2 reduction reaction[20] and oxidation of some organic substances.[21] Due to the presence of carboxy groups on the periphery, these phthalocyanines are capable of forming network polymer salts with metal cations with oxidation states of two or more. Such polymers are usually named metal-organic frameworks (MOFs).

The main aim of this study is to create a heterogeneous catalytic material based on carboxy substituted cobalt phthalocyanines by preparing MOFs that have catalytic activity in the process of oxygen activation. The activity of the obtained catalysts was studied in the oxidation reaction of 4-*tert*-butylcatechol with atmospheric oxygen.

The oxidation reaction of 4-*tert*-butylcatechol with the formation of quinone is used in medical diagnostics,[22,23] the synthesis of new organic compounds[24,25] and the production of metal complex catalysts.[26,27] In addition, this reaction has been well studied[28,29] and is often used as a model reaction to determine the catalytic activities of the new materials.[22,30] Based on this, the oxidation reaction of 4-*tert*-butylcatechol with oxygen was chosen to study the activity of the obtained catalysts.

Another method for determining catalyst activity is cyclic voltammetry. With its help, it is possible to reliably detect the formation of possible cationic and anionic forms of compounds and study the activity of the catalyst by determining the electroreduction potential of triplet oxygen.

Experimental

Materials and methods

Sodium hydroxide of analytical grade, potassium hydroxide of reagent grade, 38% hydrochloric acid of analytical grade, pyromellitic dianhydride 98%, cobalt chloride hexahydrate of analytical grade, urea of analytical grade, ammonium molebdate of reagent grade, aluminum nitrate nonahydrate of analytical grade "Sigma-Aldrich", 4-*tert*-butylcatechol ("Sigma-Aldrich"), acetone, ethanol 96% and dimethylformamide (DMF) of reagent grade were used without further purification.

UV-Vis spectra were obtained on a Shimadzu UV 2550 spectrophotometer in the wavelength range of 250-850 nm. IR spectra were recorded on an Avatar 360 Nikolet IR-Fourier spectrophotometer, USA. Mass spectra were obtained using MALDI ToF Shimadzu Axima Confidence, UK 2014.

Microphotographs were taken using a scanning electron microscope VEGA 3 SBH with an attachment for elemental analysis and a spray installation for applying carbon coating, TESCAN, Czech Republic 2016.

Phthalocyanine synthesis

The synthesis of the starting phthalocyanines was carried out according to the known method[31] with some modifications.

Cobalt tetracarboxyphthalocyanine (CoPc(COOH)$_4$). Trimellitic anhydride 5 g (23 mmol), urea 26 g (430 mmol) and ammonium molybdate 0.5 g were placed in a 250 mL round bottom flask. Mixture was heated on a hotplate at 180 °C to melt the urea, and kept at this temperature for 20 minutes until foaming stopped. Then, cobalt(II) chloride hexahydrate (2.7 g, 11.5 mmol) was added and waited for its complete dissolution. The resulting melt was placed in a microwave reactor. Irradiation was carried out in pulses (power 700 W, pulse duration 3-5 s, pause duration 10 s) for 15 min. When the melt darkened and solidified, phthalocyanine was formed. Moreover, it is necessary to stake out of the process and stop microwave exposure if excessive gas formation and foaming of the mixture.

The reaction mass was cooled to room temperature, 20% hydrochloric acid (200 mL) was added and the mixture was heated for 2 h to remove urea decomposition products. Then, a precipitate was filtered off and dried. The dry precipitate was poured into 150 mL of isopropyl alcohol, sodium hydroxide (20 g) was added and the mixture was boiled for 40 h. The reaction end was monitored by the stop of ammonia evolution. This stage is the hydrolysis of peripheral amides to form carboxyl groups (see Scheme 1).

At the end of hydrolysis, the precipitate was filtered. The powder was dissolved in a least volume of 0.2 M aqueous alkaline solution. The resulting solution was filtered, the filtrate was acidified with concentrated hydrochloric acid to a slightly acidic reaction (p*H* = 5-6), and a precipitate formed. The precipitate was separated by filtration and washed with slightly acidified hot water to remove most water-soluble admixture. The washed precipitate was again dissolved in an aqueous alkaline solution and filtered. The filtrate was acidified, a precipitate formed, which was filtered. This operation was carried out 4 times. The isolated cobalt phthalocyanine after final precipitation was filtered and washed with a small amount of water and then with isopropyl alcohol and dried at 120 °C. Yield of CoPc(COOH)$_4$: 1.23 g, 1.65 mmol (27.5% on trimellitic anhydride). *m/z* (MALDI TOF) %: 747 (100) [M^+], 702 (12) [M^+-CO_2]. IR (KBr) ν_{max} cm^{-1}: 3192 s, 2605 m and 2500 m, 1697 s. UV-Vis (H_2O) λ_{max} nm: 336, 608, 677;

Cobalt octacarboxyphthalocyanine (CoPc(COOH)$_8$) was obtained according to the previously described method for the synthesis of cobalt tetracarboxyphthalocyanine. But in this case pyromellitic dianhydride was used as the starting compound. Yield of CoPc(COOH)$_8$: 0.55 g, 0.60 mmol (11% on pyromellitic dianhydride). *m/z* (MALDI TOF) %: 925 (100) [M+2H^+], 906 (67) [M-H_2O+H^+], 888 (28) [M-2H_2O+H^+], 868 (12) [M^+-3H_2O]. IR (KBr) ν_{max} cm^{-1}: 3164 s, 2603 m and 2498 m, 1705 s. UV-Vis (H_2O) λ_{max} nm: 336, 619, 685.

MOF fabrication

Preparation of MOF based on CoPc(COOH)$_4$ (CoPc(COO)$_4$Al). To obtain a metal-organic framework, 100 mg (0.13 mmol) of CoPc(COOH)$_4$ was added to a 100 mL round-bottom flask and dissolved in a least volume of DMF (50–70 mL). Then aluminum nitrate nonahydrate (50 mg, 0.13 mmol) was added and the mixture was heated at 120°C for 1.5–2 h. The end of the reaction was indicated by the discoloration of the solution and the formation of a precipitate. It was separated by centrifugation at 3000 rpm for 5 min. Powder was washed with 30 mL of DMF until the fugate was completely discolored, then precipitate was washed with water and acetone. The resulting product was dried at 80°C. Yield of CoPc(COO)$_4$Al: 70.5 mg (70% on CoPc(COOH)$_4$). IR (KBr) ν_{max} cm^{-1}: 540 m, 650 m. UV-Vis (H_2O) λ_{max} nm: 636, 689.

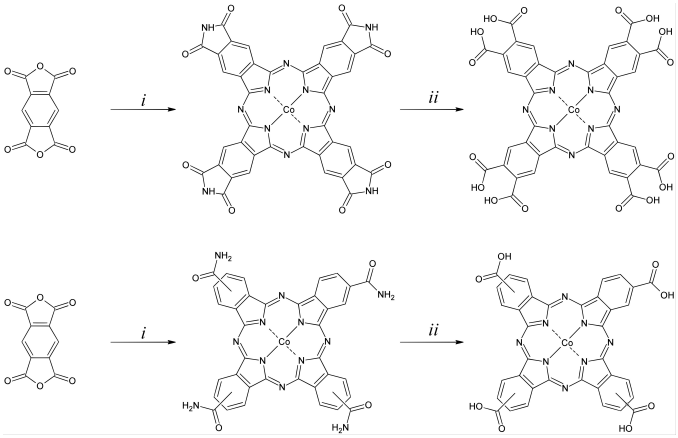

Scheme 1. Synthesis of cobalt tetra- and octacarboxy-phthalocyanines. *i* – $CoCl_2$, urea, microwave heating to 200°C; *ii* – isopropanol, KOH, reflux, then HCl.

Preparation of MOF based on CoPc(COOH)$_8$ (CoPc(COO)$_8$H$_4$Al$_2$). The preparation of this material was carried out according to the method described above for CoPc(COO)$_4$Al using 81 mg (0.22 mmol) of aluminum nitrate nonahydrate and 100 mg (0.11 mmol) of CoPc(COOH)$_8$. Yield of CoPc(COO)$_8$H$_4$Al$_2$: 82.6 mg (82% on CoPc(COOH)$_8$). IR (KBr) ν_{max} cm^{-1}: 540 m, 650 m. UV-Vis (H_2O) λ_{max} nm: 623, 680.

MOF Catalytic activity in the 4-tert-butylcatechol oxidation reaction

25 mL of 4-*tert*-butylcatechol solution in ethanol with a concentration of 10^{-3} M was added to a thermostated flask with a capacity of 100 mL and the initial absorption spectrum was recorded. Then 1 mg of the MOF was placed into the flask. The samples were taken to detect accumulation of quinone by recording the UV-Vis spectrum every 5 min. The kinetic experiment was carried out at temperatures in the range of 40-60°C with steps of 5°C.

Cyclic voltammetry

Electrochemical measurements were performed by the method[45] in the three-electrode cell YASE-2. A saturated silver chloride electrode (Ag/AgCl) and a platinum electrode were used as the reference and counter electrodes, respectively. The working electrode was a graphite one. The working surface (0.64 cm^2) was deposited with a layer (0.2–0.3 mm) of an active mass, which was prepared in an ethyl alcohol, involved the carbon support (TEC - technical elemental carbon P-514 (State standard 7885-86) with the ash content 0.45%), the fluoroplastic suspension (6% FP-4D) and the Pc in weight ratio 7:2:1.

The electrolyte was first deaerated with argon (99.99%) by bubbling at a rate of 20 mL/min for 40 minutes. Then, the redox processes on the surface of the original and phthalocyanine-modified electrodes were studied. The working electrode was

dipped in the electrolyte, and cyclic voltammograms were recorded in the potential range from 0.5 to –1.5 V. When measurements in an argon atmosphere were completed, oxygen gas was bubbled into the electrolyte.

The measurements were carried out by using the potentiostat-galvanostat «J-31P» (Electrochemical Instruments, Russia). Potentials of cathodic (E_c) and anodic (E_a) peaks were fixed with the accuracy of ±0.01 V. The relative error did not exceed 3–5% in determining the values of redox potentials.

Calculation Method

Geometries of both MOF were simulated and optimized by HyperChem 8.0.7 using of MM+ method. Data visualization was performed by the Mercury 2023.3.0.

Results and Discussion

Dye and MOF spectroscopic analyses

The presence of phthalocyanine can be confirmed by UV-Vis spectra with sufficient accuracy. In addition, the spectra can be used to determine the electronic state of molecules (cation, anion or radical, *etc*.) and supramolecular structures (formation of aggregates or donor-acceptor complexes).

UV-Vis spectra were obtained for the original Pc and MOF and are shown in Figure 1. The original cobalt phthalocyanines in an aqueous alkaline solution are in a monomolecular form, this is evident from the intense Q-bands at 677 nm (a) and 685 nm (b) and the absence of additional bands in the spectra.

The baseline rise is observed on the spectrum in a blue region of the of $CoPc(COOH)_4$ (Figure 1(a)), which indicates the presence of a suspension of undissolved phthalocyanine. This fact is due to the poor solubility of $CoPc(COOH)_4$ in an aqueous alkaline solution.

MOF is insoluble in an aquatic medium and exists in a suspension form. This fact is confirmed by the rise of the baseline in the blue region of the spectrum. In addition, the appearance of new absorption bands with maxima at 631 nm (a) and 623 nm (b) shifted hypsochromically relative to the main Q-peak is observed, which indicates the pseudo T-type aggregated formation.[32] From the structures of the MOFs (see below) it is clear that the relative position of the phthalocyanine molecules exactly corresponds to the position of the molecules during T-type aggregation.

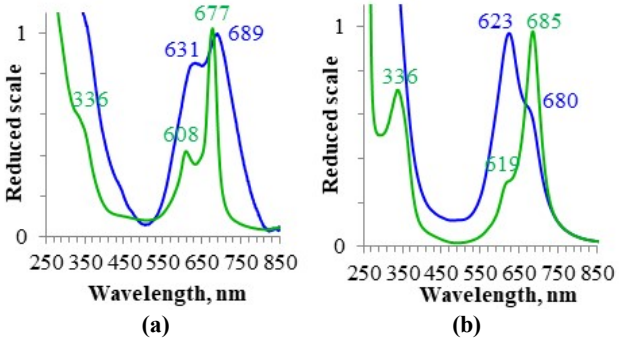

Figure 1. UV-Vis spectra of cobalt tetra- (a) and octacarboxyphthalocyanines (b) in aqueous alkaline (green lines), and MOF based on them in water (blue lines).

Furthermore, from the absorption spectra it is clear that for the $CoPc(COO)_4Al$ the intensity of the new band (at 631 nm) is lower than the Q-peak and, on the contrary, for the $CoPc(COO)_8H_4Al_2$ it is higher. From which we can conclude that there is a stronger interaction in the case of the $CoPc(COO)_8H_4Al_2$, which corresponds to the electronic transition responsible for the intermolecular interaction of T-aggregates. This consequence is also confirmed by the structures of MOFs, in which in the case of the $CoPc(COO)_8H_4Al_2$ the cobalt octacarboxyphthalocyanines touch with their side faces, which enhances the interaction and increases the probability of an electronic transition, while in the case of the $CoPc(COO)_4Al$ the molecules touch only at the corners – carboxyl groups.

A large amount of information can also be obtained from IR spectra. FTIR of all compounds in KBr tablets are presented in Figure 1S.

Bands at 3192 and 3164 cm^{-1} are observed in the IR spectra of both phthalocyanines, which are responsible for the stretching vibrations of the O-H bond in the carboxyl group. Bands at 1697 and 1705 cm^{-1} correspond to the stretching vibrations of C=O. Also, 2600 and 2500 cm^{-1} are observed, which relate to proton vibrations in the structure of six-membered carboxylic acid dimers.[33]

The bands at 3192 and 3164 cm^{-1} are absent for MOFs. Moreover, in the case of $CoPc(COO)_8H_4Al_2$, the band at 1705 also is decreased, that indicates the manifestation of the bidentate type of binding of the carboxyl group with aluminum atoms. In addition, the appearance of a wide band in the region of 400–700 cm^{-1} is observed. The band at 540 cm^{-1} corresponds to the stretching vibration of Al-O in the AlO_6[34] octahedron and at 650 cm^{-1} corresponds to the bending vibration of O-Al-O in the aluminum oxide cluster.[35-37]

MOF Catalytic activity in the 4-tert-butylcatechol oxidation reaction

A catalytic reaction of 4-*tert*-butylcatechol oxidation by atmospheric oxygen was carried out in order to determine the activity of MOF in the process of oxygen activation. For example, spectral changes in catalytic experiment with $CoPc(COO)_8H_4Al_2$ as a catalyst and reaction medium temperature of 50°C are shown in Figure 2.

Based on the spectral data, kinetic dependences of quinone accumulation *vs* time were constructed used known extinction coefficient[38,39] (Figure 3).

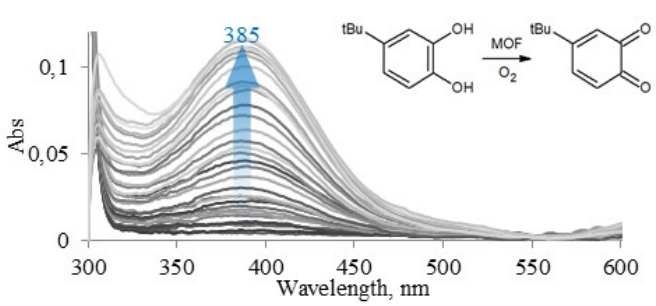

Figure 2. UV-Vis spectra changes under the quinone accumulation.

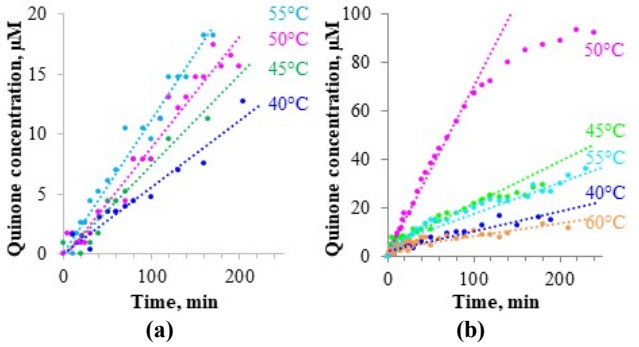

Figure 3. Kinetic dependences of quinone accumulation *vs* time at different temperatures; $CoPc(COO)_4Al$ (a) and $CoPc(COO)_8H_4Al_2$ (b) were used as a catalyst.

From the given kinetic dependencies, it can be noted that the quinone accumulation rate *vs* time is linearized in terms of concentration *vs* time. This behavior indicates the nil order (n = 0) of the process and, as a consequence, the non-chemical stage is limiting. Diffusion of substances in the volume of solution, diffusion inside the catalyst pores, adsorption and desorption are such stages for heterogeneous catalysis.

Limitation of diffusion in the solution volume is eliminated by intensive mixing. The diffusion of compounds into the catalyst cavity usually depends on the molecules movement speed and, as a consequence, on temperature. In the shown kinetic dependencies, it can be seen that with increasing temperature the reaction rate increases, which indicates that this stage is limited in the entire process.

Moreover, with an increase in temperature above 50 °C for $CoPc(COO)_8H_4Al_2$, a decrease in activity is observed, that can be caused by decreasing concentration of the dissolved oxygen due to heating of the solvent. In this case, the stage of oxygen absorption from the air begins to limit.

The operating conditions and data obtained during the catalytic experiment are presented in Table 1.

The auto-oxidation of 4-*tert*-butylcatechol and its oxidation by starting cobalt phthalocyanines were studied under similar conditions. The spectral changes recorded during both processes did not exceed the instrumental error, which may indicate very low rates of accumulation of the reaction product.

During the analysis of literature data,[22,29,40,41] the mechanism of the first cycle of catalytic oxidation of 4-*tert*-butylcatechol was adapted to the catalysts under study (Figure 4), where the active center is cobalt phthalocyanine.

Table 1. Data on the activity of MOFs in the catalytic reaction.

	$CoPc(COO)_4Al$				$CoPc(COO)_8H_4Al_2$			
Temperature, °C	40	45	50	55	40	45	50	55
Max rate, μM/min	0.055	0.074	0.092	0.111	0.084	0.176	0.690	0.130
n(BC)/n(MOF)	25							
Quinone yield (per 160 min), %	0.6	0.8	1.2	1.2	1	2	6.8	1.6

The Table 1 shows that the conversion of 4-*tert*-butylcatechol to quinone does not exceed 10%. The fact is that during the process of oxidation of 4-*tert*-butylcatechol with atmospheric oxygen, hydrogen peroxide is released on the catalyst (Figure 4). Hydrogen peroxide is capable of participating in reactions of further oxidation of quinone into products that do not have spectral activity (Figure 5). This fact has been well studied and described.[5]

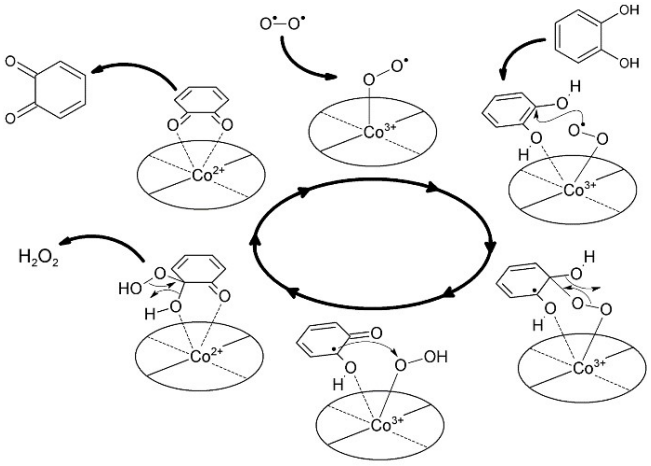

Figure 4. The catalytic action mechanism of cobalt phthalocyanine in the oxidation process of 4-*tert*-butylcatechol by atmospheric oxygen (^{t}Bu substituents are omitted to simplify the scheme).

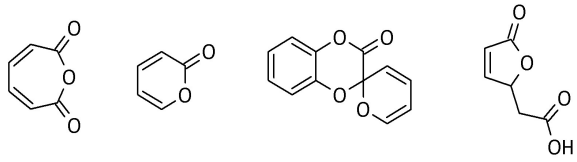

Figure 5. Quinone oxidation reaction products.

Cyclic voltammetry

CV analysis was carried out to confirm the catalytic activity of the studied materials in the oxygen reduction reaction. It should be noted that the anode and cathode maxima were not observed in the studied potential range in the case of an active mass without phthalocyanine. On the contrary, anode and cathode maxima appeared when phthalocyanine was introduced into the active mass. At the same time, processes, corresponding to the reduction and oxidation of both ligands and the cobalt ion, were observed. It has been determined that the cobalt(II) tetra- and octacarboxyphthalocyanine have similar electrochemical behavior (Table 2).

The process of reduction/oxidation of cobalt ion (Co^{2+} ⇆ Co^{3+}) was observed on the CV curves (Figure 6) in region I (0.30 ÷ 0.05 V), which is in agreement with literature data:[42-47]

$$\underset{\textit{neutral form}}{Co^{+2}Pc(COOH)_n} \leftrightarrows \underset{\textit{monocationic}}{Co^{+3}Pc(COOH)_n}$$

where *n* = 4 or 8.

Table 2. Potentials of redox process (υ = 0.02 V/s).

Compound	$Co^{3+} \leftrightarrows Co^{2+}$ $^{a}Co^{2+} \leftrightarrows Co^{1+}$			Process $L \rightarrow L^{-\bullet}$			Process $L^{-\bullet} \rightarrow L^{2-}$		
	E_c, V	E_a, V	$E_{red/ox}$, V	E_c, V	E_a, V	$E_{red/ox}$, V	E_c, V	E_a, V	$E_{red/ox}$, V
CoPc[48]		*	0.11 -0.54[a]		*	-0.82		*	
$CoPc(COOH)_4$ [49]		*	0.23 -0.51[a]		*	-1.07		*	
$CoPc(COOH)_4$ [47]	0.11	0.20	0.16	-1.07	-0.60	-0.84	-1.23	-1.15	-1.19
$CoPc(COOH)_4$	0.12 -0.61[a]	0.28 -0.35[a]	0.20 -0.48[a]	-1.08	-0.60	-0.84	-1.29	-1.15	-1.22
$CoPc(COOH)_8$	0.11 -0.59[a]	0.24 -0.41[a]	0.18 -0.50[a]	-1.10	-0.62	-0.86	-1.29	-1.16	-1.23
$CoPc(COO)_4Al$	0.14 -0.61[a]	0.27 -0.42[a]	0.21 -0.52[a]	-1.09	-0.61	-0.85	-1.28	*	*
$CoPc(COO)_8Al_2$	0.14 -0.56[a]	0.25 -0.44[a]	0.19 -0.50[a]	-1.09	-0.62	-0.86	-1.29	*	*
TEC	**	**	**	**	**	**	**	**	**

* – not determined
** – without transition

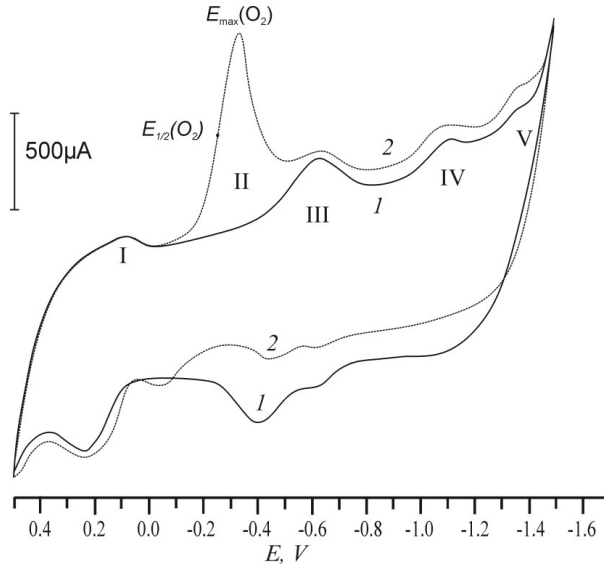

Figure 6. *I,E*-curves for an electrode modified with $CoPc(COOH)_8$. υ = 0.02 V/s in 0.1M KOH. *1* – Ar; *2* – O_2 (maximum saturation).

Cathode and anodic current maxima are observed in region II (0.0 ÷ –0.4 V) and disappear when argon is bubbled through the electrolyte. The maximum value of the oxygen electroreduction current corresponds to the potential $E_{max}(O_2)$. Therefore, the transitions relate to the process of oxygen reduction/oxidation. In addition, the absence of these in curve *1* indicates complete deaeration of the electrolyte and removal of oxygen from the surface of the electrode and catalyst.

The process of adding an electron to a neutral molecule with localization of the electron on the metal was observed in the potential region III (–0.30 ÷ –0.70 V):

$$\underset{\textit{neutral form}}{Co^{+2}Pc(COOH)_n} \leftrightarrows \underset{\textit{monoanion radical}}{[Co^{+1}Pc(COOH)_n]^{-*}}$$

The electroreduction processes with the addition of one electron to the π-electron ligand system was observed in the potential regions IV and V (–0.60 — –1.10 V and –1.10 — –1.40):

$$\underset{\textit{monoanion radical}}{[Co^{+1}Pc(COOH)_n]^{-*}} \leftrightarrows \underset{\textit{dianion}}{[Co^{+1}Pc(COOH)_n]^{-2}} \leftrightarrows \underset{\textit{trianion}}{[Co^{+1}Pc(COOH)_n]^{-3}}$$

The electrochemical stages sequence is the same for the $CoPc(COOH)_4$ and $CoPc(COOH)_8$. The potential values of the redox processes and their reversibility in an inert medium are close within the error.

The transition $Co^{3+} \leftrightarrows Co^{2+}$ was recorded for MOF – $CoPc(COO)_4Al$ and $CoPc(COO)_8H_4Al_2$ at $E_{red/ox}$ = 0.21 and 0.19 V, respectively. The value of this transition is shifted in the positive direction by 80–100 mV compared to unsubstituted[48] and carboxysubstituted cobalt phthalocyanines. The electroreduction of the metal ion ($Co^{2+} \leftrightarrows Co^{1+}$) and ligation under the conditions under consideration occurs at the same potentials as for catalysts without aluminum.

A new cathode wave is observed for the studied complexes in the region of 0.0 ÷ –0.4 V when the electrolyte is saturated with oxygen, which corresponds to the oxygen reduction reaction (ORR) process. A significant shift (100–150 mV) of the potentials $E_{max}(O_2)$ and $E_{1/2}(O_2)$ to the region of positive potential values was observed for all studied catalytic systems. This indicated a decrease in the polarization of the cathodic reaction. Current values at potential $E_{max}(O_2)$ were measured at different scan rates. A linear dependence in I_p *vs* $\sqrt{v}$ coordinates was observed in all cases in the range from 0.005 to 0.020 V/s. The resulting

pattern indicates diffusion control of this process and allows the use of the Randles-Sevcik Equation 1[46] to calculate the effective number of electrons (n):

$$I_p = 272\sqrt{n^3}\, S\, C_a \sqrt{v\, D_a},$$

where I_p – maximum current, A; S – electrode surface, cm^2; C_a – solubility of substance A, mol/L; D_a – diffusion coefficient, cm^2/s; υ – scanning speed, V/s. The following values of the parameters included in the equation were used in the calculations: S = 0.64 cm^2; $C(O_2) = 1.2\cdot10^{-3}$ mol/L; $D(O_2) = 1.9\cdot10^{-5}$ cm^2/s.

Analysis of the values of the effective number of electrons n (Table 3), calculated using the Rendles-Sevcik equation,[41] showed that for all studied catalysts n lies in the range of 3.0÷3.9. Therefore, the ORR process for the studied catalysts can proceed in parallel using both the 2 and 4 electronic mechanisms with the formation of oxygen-containing intermediates, as described in [44, 50-52].

An increase in the values of n and in the shift of the wave of electroreduction of molecular oxygen [$E_{1/2}(O_2)$] to the region of positive potential values, compared with the system without a catalyst ($E_{1/2}(O_2)$ = -0.35 V, Table 3) indicates the participation of the studied complexes in electrocatalysis of the process under consideration. An decrease in the number of carboxy groups in phthalocyanine and the MOFs formation lead to an increase in activity. The electrocatalytic activity of the studied compounds in the ORR increases in the order: CoPc[48] < $CoPc(COOH)_8$ < $CoPc(COOH)_4$ (Table 3).

Table 3. ORR parameters.

Compound	$E_{max}(O_2)$, V	$E_{1/2}(O_2)$, V	n
CoPc [48]	*	-0.26	*
$CoPc(COOH)_4$ [49]	*	-0.25	*
$CoPc(COOH)_4$ [47]	*	-0.20	2.5
$CoPc(COOH)_4$	-0.25	-0.17	3.0
$CoPc(COOH)_8$	-0.31	-0.24	3.9
$CoPc(COOH)_4Al_2$	-0.26	-0.20	3.9
$CoPc(COOH)_8Al_2$	-0.28	-0.23	3.9
Elemental carbon	-0.39	-0.35	2.0

* – not determined

SEM and elemental analysis

For the studied MOFs, microphotographs of the powders were obtained and their X-ray fluorescence analysis was carried out to get closer to understanding the structure of the MOFs. Using SEM, it is possible to determine whether crystals have formed and what shape they are, so that one can indirectly judge the symmetry of the crystal cell. Microphotographs of MOFs are presented in Figure 7.

Table 4. Elemental composition of the MOFs based on cobalt carboxyphthalocyanines (calculated/**found**).

	$CoPc(COO)_4Al$	$CoPc(COO)_8H_4Al_2$
C	36/**37**	40/**40.1**
N	8/**9.4**	8/**8.2**
O	8/**8.8**	18.7/**17.5**
Al	1/**1.1**	2/**1.9**
Co	1/**1**	1/**1**

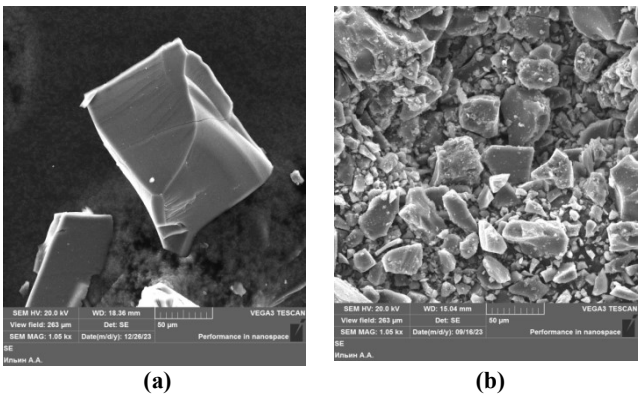

(a) **(b)**

Figure 7. Microphotographs of $CoPc(COO)_4Al$ (a) and $CoPc(COO)_8H_4Al_2$ (b).

Microphotographs clearly show crystalline formations. The crystals do not have a clear shape, but some of them have the outline of a cube, namely the perpendicularity of adjacent faces and the formation of cubic vertices. This may lead to a search for 3D cubic or 2D square structures.

X-ray fluorescence analysis made it possible to determine the Co:Al ratio in MOFs. The results of elemental analysis are presented in Table 4 (calculated /determined) in the form of a molar ratio of the element to cobalt since the number of cobalt atoms is numerically equal to the number of phthalocyanine molecules.

It is important to note that when studying the elemental composition of the organic part, it is necessary to take into account that carbon tape was used as a substrate, which could introduce an error in the measurements.

The Co:Al ratios were clearly defined, namely for $CoPc(COO)_4Al$ it is 1:1, for $CoPc(COO)_8H_4Al_2$ it is 1:2. These ratios will allow us to get closer to the structure of the MOFs being studied.

Structure

In the search for a suitable structure of MOFs, a large amount of literature was analyzed, which describe MOFs containing organic ligands with carboxyl groups and aluminum as binding components. Often these articles deal with small linkers, for example phthalic acid,[53] pyromellitic acid,[54] metallocenes,[55] acetylenedicarboxylic acid,[56] *etc*.

MOFs based on metallophthalocyanines have also been found, but they contain hydroxo-[57] and amino-[58] groups on the periphery. Since these groups are in the plane of the macrocycle and MOFs based on them form 2D structures.

A search for the structure in the literature did not yield significant results. We decided to independently determine the structure of the studied MOFs. Since the phthalocyanine molecule is flat, the main contribution to the MOFs structure will be made by the aluminum oxide cluster.

Aluminum ions can have coordination number of 4 and 6. The coordination number of aluminum in the composition of an aluminum oxide cluster can be easily determined from the IR spectrum of the compound[22,40,41] containing these clusters. In the given spectra for MOFs (Figure S1), a new broad band appears in the region of 550-600 cm^{-1}, which corresponds to the vibration of the Al-O

bond in an aluminum oxide cluster, while aluminum in such a cluster has a coordination number of 6.[40]

Also, according to the literature,[53,54,60-62] possible aluminum-oxide clusters were found that can be formed by aluminum with a coordination number of 6. The structures of these clusters are shown in Figure 8.

Long-chain clusters (Figure 8c and d) are not suitable in this case, since phthalocyanine molecules have a large volume and will not be able to form such a dense packing.

Based on experimental data on optimizing the ratio of aluminum salt and phthalocyanine in the reaction of MOF formation, it was found that the maximum yield, tending to be quantitative, was achieved at Al:Pc molar ratio 1:1 for $CoPc(COO)_4Al$ and 1:2 for $CoPc(COO)_8H_4Al_2$.

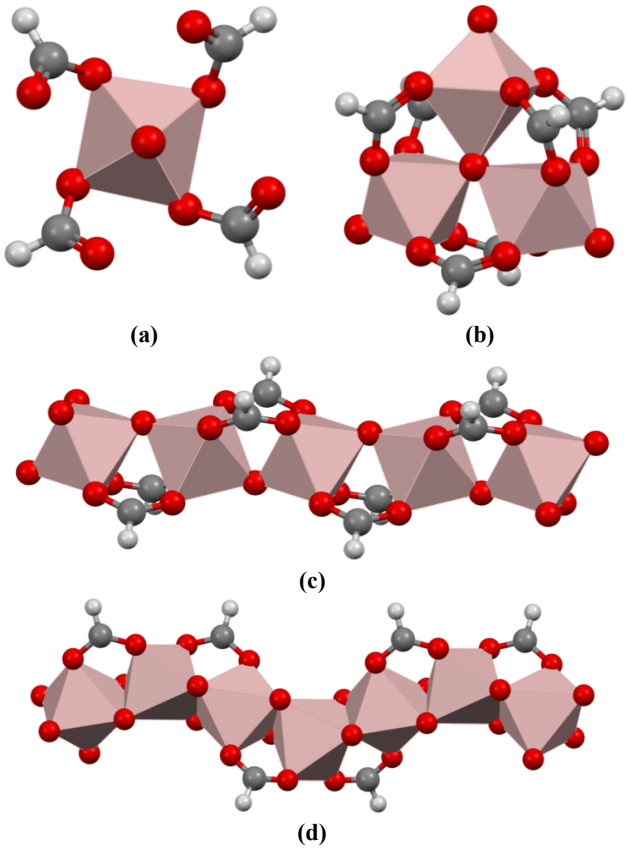

Figure 8. Structures of possible aluminum oxide clusters (atoms are shown as balls: red - oxygen, gray - carbon, white - organic linker, and in the center of the bipyramids are aluminum atoms).

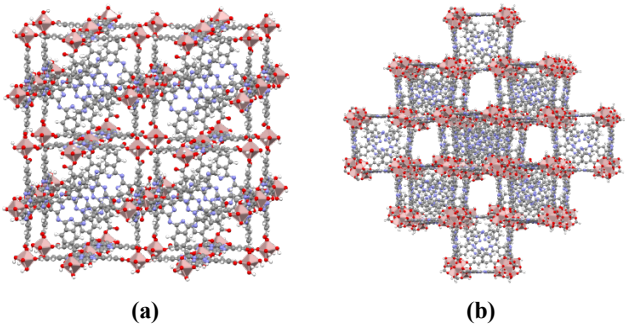

Figure 9. Hypothesized structure of the studied MOFs: $CoPc(COO)_4Al$ (a) and $CoPc(COO)_8H_4Al_2$ (b).

Quantum chemical modeling of the possible structures of the studied MOFs containing carboxyphthalocyanine as a linker and aluminum oxide clusters yielded only one structure for $CoPc(COO)_4Al$ with clusters (Figure 8a) and one for $CoPc(COO)_8H_4Al_2$ with clusters (Figure 8b), presented in Figure 9. For ease of modeling and perception, cobalt atoms in both cases and four carboxy groups for cobalt octacarboxyphthalocyanine were removed.

The resulting structures confirm the data obtained from the heterogeneous catalytic experiment on the oxidation of 4-*tert*-butylcatechol with atmospheric oxygen catalyzed by the studied MOFs. Namely, for $CoPc(COO)_4Al$, a much smaller pore size is observed compared to $CoPc(COO)_8H_4Al_2$, which will greatly reduce the efficiency of such a heterogeneous catalyst.

Moreover, phthalocyanines are stimulated to form precisely these structures by their presence in the form of dimers of carboxylic acids. In this case, during the formation of MOF, the interaction of two structures occurs: an aluminum ion and a dimer of carboxylic acids – phthalocyanine. During the incorporation of the Al^{3+} ion, the dimer is bent and the structures shown in Figure 9 are formed.

Conclusions

Cobalt tetra- and octacarboxyphthalocyanines were synthesized. Metal-organic frameworks were obtained based on them and the optimal Pc:Al ratios were experimentally determined, which were 1:1 for $CoPc(COO)_4Al$ and 1:2 for $CoPc(COO)_8H_4Al_2$. The ability of these compounds to activate oxygen was studied using kinetics experiments and cyclic voltammetry methods. A catalytic experiment was carried out on the oxidation of 4-*tert*-butylcatechol with atmospheric oxygen, catalyzed by the MOFs. As a result, it was shown that the limiting stage of the process is the diffusion of molecules inside the pores of the MOFs catalyst structure. At the same time, for $CoPc(COO)_8H_4Al_2$ there is a strong dependence of catalytic activity on temperature, in contrast to $CoPc(COO)_4Al$. This fact indicates that $CoPc(COO)_8H_4Al_2$ has a larger pore size compared to $CoPc(COO)_4Al$.

ORR was also carried out on a graphite electrode supported by phthalocyanines. The results of the experiment demonstrated the opposite effect of activity. The half-wave potential of oxygen reduction for $CoPc(COOH)_4$ was -0.17 V, and for $CoPc(COOH)_8$ was -0.24 V. This fact indicates a greater activity of $CoPc(COOH)_4$ in the ORR.

The discrepancies in experimental data were associated with the large influence of the studied MOFs structure on the process of oxygen activation in different experiments. Using a number of empirical and literary data, probable structures of MOFs have been proposed, which are indirectly confirmed by experimental data.

Acknowledgments. The work was carried out within the framework of the State assignment, topic No. FZZW-2023-0009. The study was carried out using the resources of the Center for Collective Use of Scientific Equipment at ISUCT (with the support of the Ministry of Education and Science of Russia, agreement No. 075-15-2021-671).

Conflict of interests. Authors have no conflict of interests to declare.

References

1. Lange J.P. *Nature Catalysis* **2021**, *4*, 186–192. DOI: 10.1038/s41929-021-00585-2.
2. de Vries J.G., Jackson S.D. *Catal. Sci. Technol.* **2012**, *2*, 2009–2009. DOI: 10.1039/C2CY90039D.
3. Cornils B., Herrmann W.A. *J. Catal.* **2003**, *216*, 23–31. DOI: 10.1016/S0021-9517(02)00128-8.
4. Beller M., Renken A., van Santen R.A. *Catalysis: from Principles to Applications.* Weinheim: Wiley-VCH Verlag. **2012**, 642 p. ISBN: 9783527323494.
5. *Vanadium Catalysis* (Sutradhar M., da Silva J.A.L., Pombeiro A.J.L., Eds.) Royal Society of Chemistry, Cambridge, UK, **2020**. ISBN: 978-1-83916-088-2, ISSN: 1757-6733.
6. Sutradhar M. *Catalysts* **2020**, *10*, 1429. DOI: 10.3390/catal10121429.
7. Shi J., Wang Y., Yang W., Tang Y., Xie Z. *Chem. Soc. Rev.* **2015**, *44*, 8877–8903. DOI: 10.1039/C5CS00626K.
8. Wei D., Sadek O., Dorcet V., Roisnel T., Darcel C., Gras E., Clot E., Sortais J.-B. *J. Catal.* **2018**, *366*, 300–309. DOI: 10.1016/j.jcat.2018.08.008.
9. Seck C., Mbaye M.D., Gaillard S., Renaud J.L. *Adv. Synth. Catal.* **2018**, *360*, 4640–4645. DOI: 10.1002/adsc.201800924.
10. Kar S., Sen R., Kothandaraman J., Goeppert A., Chowdhury R., Munoz S.B., Haiges R., Prakash G.K.S. *J. Am. Chem. Soc.* **2019**, *141*, 3160–3170. DOI: 10.1021/jacs.8b12763.
11. Kumar A., Daw P., Milstein D. *Chem. Rev.* **2021**, *122*, 385–441. DOI: 10.1021/acs.chemrev.1c00412.
12. Chen Q., Yin Q., Dong A., Gao Y., Qian Y., Wang D., Dong M., Shao Q., Liu H., Han B.H., Ding T., Guo Z., Wang N. *Polymer* **2019**, *169*, 255–262. DOI: 10.1016/j.polymer.2019.02.056.
13. Huang K., Zhang J. Y., Liu F., Dai S. *Acs Catalysis*. **2018**, *8*, 9079–9102. DOI: 10.1021/acscatal.8b02151.
14. Sorokin A.B. *Chem. Rev*. **2013**, *113*, 8152–8191. DOI: 10.1021/cr4000072.
15. Szymczak J., Kryjewski M. *Materials* **2022**, *15*, 2532. DOI: 10.3390/ma15072532.
16. Liu W., Wang K., Wang C., Liu W., Pan H., Xiang Y., Qi D., Jiang, J. *J. Mater. Chem. A* **2018**, *6*, 22851–22857. DOI: 10.1039/C8TA08173E.
17. Wang H.G., Wu Q., Cheng L., Chen L., Li M., Zhu G. *Energy Storage Materials* **2022**, *52*, 495–513. DOI: 10.1016/j.ensm. 2022.08.022.
18. Ji W., Wang T.X., Ding X., Lei S., Han B.H. *Coord. Chem. Rev*. **2021**, *439*, 213875. DOI: 10.1016/j.ccr.2021.213875.
19. Zhang Z., Wang W., Wang X., Zhang L., Cheng C., Liu X. *Chem. Eng. J.* **2022**, *435*, 133872. DOI: 10.1016/j.cej.2021.133872.
20. Huang S., Chen K., Li T.T. *Coord. Chem. Rev.* **2022**, *464*, 214563. DOI: 10.1016/j.ccr.2022.214563.
21. Mackintosh H.., Budd P.M., McKeown, N.B. *J. Mater. Chem.* **2008**, *18*, 573-578. DOI: 10.1039/B715660J.
22. Castro K.A., Figueira F., Paz F.A.A., Tomé J.P., da Silva R.S., Nakagaki S., Neves M.G.P.M.S., Cavaleiro J.A.S., Simões M. M. *Dalton Trans.* **2019**, *48*, 8144–8152. DOI: 10.1039/C9DT00378A.
23. Lebedev A.V., Ivanova M.V., Timoshin A.A., Ruuge E.K. *Biomedical Chemistry [Biomed. Khimiya]* **2008**, *54*, 687–695.
24. Kashiwagi T., Amemiya F., Fuchigami T., Atobe M. *Chem. Commun*. **2012**, *48*, 2806–2808. DOI: 10.1039/C2CC17979B.
25. Yadoung S., Shimizu S., Hongsibsong S., Nakano K., Ishimatsu R. *Heliyon* **2023**, *9*, e21722. DOI: 10.1016/j.heliyon.2023.e21722.
26. Zherebtsov M.A., Arsenyev M.V., Baranov E.V., Chesnokov S.A. *J. Struct. Chem*. **2023**, *64*, 2051–2062. DOI: 10.1134/S002247662311003.
27. Zhou B., Bedajna S., Gabbaï F.P. *Chem. Commun*. **2024**, *60*, 192–195. DOI: 10.1039/D3CC04942F.
28. Tyson C. A., Martell A.E. *J. Phys. Chem.* **1970**, *74*, 2601–2610. DOI: 10.1021/j100707a004.
29. Lebedev A.V., Ivanova M.V., Ruuge E.K. *Biophysics* **2011**, *56*, 188–193. DOI: 10.1134/S0006350911020187.
30. Salonen P., Savela R., Peuronen A., Lehtonen A. *Dalton Trans.* **2021**, *50*, 6088–6099. DOI: 10.1039/D1DT00419K.
31. Jin L., Chen W., Chen, D. *J. Serb. Chem. Soc.* **2012**, *77*, 1223–1237. DOI: 10.2298/JSC110710026J.
32. Valkova L.A., Glibin A.S., Koifman O.I. *Macroheterocycles* **2011**, *3*, 222–226. DOI: 10.6060/mhc2011.3.13.
33. Giricheva N.I., Syrbu S.A., Bubnova K.E., Fedorov M.S., Kiselev M.R., Girichev G.V. *J. Mol. Liq.* **2019**, *277*, 833–842. DOI: 10.1016/j.molliq.2019.01.029.
34. Chowdhuri R.A., Takoudis C.G., Klie R.F., Browning N.D. *Appl. Phys. Lett.* **2002**, *80*, 4241–4243. DOI: 10.1063/1.1483903.
35. Kim Y.C., Park H.H., Chun J.S., Lee W.J. *Thin Solid Films* **1994**, *237*, 57–65. DOI: 10.1016/0040-6090(94)90238-0.
36. Dhonge B.P., Mathews T., Sundari S.T., Thinaharan C., Kamruddin M., Dash, S., Tyagi A.K. *Appl. Surf. Sci*. **2011**, *258*, 1091–1096. DOI: 10.1016/j.apsusc.2011.09.040.
37. Chowdhuri A.R., Takoudis C.G. *Thin Solid Films* **2004**, *446*, 155–159. DOI: 10.1016/S0040-6090(03)01311-7.
38. Rescigno A., Sanjust E., Pedulli G.F., Valgimigli L. *Anal. Lett.* **1999**, *32*, 2007–2017. DOI: 10.1080/00032719908542948.
39. Stunnenberg F., Cerfontain H., Rexwinkel R.B. *Red. Trav. Chim. Pays-Bas*. **1992**, *111*, 438–447. DOI: 10.1002/recl.19921111005.
40. Lebedev A.V., Ivanova M.V., Timoshin A.A., Ruuge E.K. *ChemPhysChem* **2007**, *8*, 1863–1869. DOI: 10.1002/cphc.200700296.
41. Nishiura T., Ohta T., Ogura T., Nakazawa J., Okamura M., Hikichi S. *Molecules* **2022**, *27*, 6416. DOI: 10.3390/molecules27196416.
42. Mayranovskiy V.G. In: *Porphyrins: Spectroscopy, Electrochemistry, Application* (Enikolopyan N.S., Ed.) Moscow, **1987**. pp. 127–181 [В кн.: *Порфирины: спектроскопия, электрохимия, применение* (Ениколопян Н.С., ред.) М.: Наука, **1987**. с. 127–181].
43. Kadish K.M., Caemelbecke E.V., Royal G. In: *The Porphyrin Handbook, Vol. 8* (Kadish K.M., Ed.) San Diego, **2000**. p. 1–114.
44. Tarasevich M.R., Radyushkina K.A., Bogdanovskaya V.A. *Electrochemistry of porphyrins*. Moscow: Nauka, **1991**. 312 p. [Тарасевич М.Р., Радюшкина К.А., Богдановская В.А. *Электрохимия порфиринов*. М.: Наука, **1991**. 312 с.].
45. Tesakova M.V., Noskov A.V., Bazanov M.I., Berezina N.M., Parfenyuk V.I. *Russ. J. Phys. Chem. A*. **2012**, *86*, 9–13. DOI: 10.1134/S0036024411120326.
46. Bazanov M.I., Filimonov D.A., Volkov A.V., Koifman O.I. *Macroheterocyclic Compounds: Electrochemistry, Electrocatalysis, Thermochemistry*. Moscow, **2016**. 320 p. [Базанов М.И., Филимонов Д.А., Волков А.В., Койфман О.И. *Макрогетероциклические соединения: Электрохимия, электрокатализ, термохимия.* М.: ЛЕНАНД, **2016**. 320 с].
47. Berezina N.M., Bazanov M.I., Maizlish V.E. *Russ. J. Electrochem*. **2018**, *54*, 873–878. DOI: 10.1134/S1023193518130074.
48. Bazanov M.I., Petrov A.V., Zhutaeva G.V. *et al. Russ. J. Electrochem.* **2004**, *40*, 1198–1204. DOI: 10.1023/B:RUEL.0000048654.68212.1e.
49. Bazanov M.I., Berezina N.M., Kokorin M.S., Semeikin A.S., Petrova D.V. *ChemChemTech* **2023**, *66*, 46–55. DOI: 10.6060/ivkkt.20236609.6853.
50. Komarova N.S., Konev D.V., Kotkin A.S., Kochergin V.K., Manzhos R.A., Krivenko A.G. *Mendeleev Commun.* **2020**, *30*, 472–473. DOI: 10.1016/j.mencom.2020.07.021.

51. Krivenko A.G., Manzhos R.A., Kotkin A.S., Kochergin V.K. *Russ. J. Electrochem*. **2020**, *56*, 418–421. DOI: 10.1134/S1023193520050079.
52. Sani F.M., Nesic S.A. *Electrochim. Acta* **2024**, *477*, 143766. DOI: 10.1016/j.electacta.2024.143766.
53. Reinsch H., De Vos D., Stock N. *Z. Anorg. Allg. Chem.* **2013**, *639*, 2785–2789. DOI: 10.1002/zaac.201300357.
54. Volkringer C., Loiseau T., Guillou N., Férey G., Haouas M., Taulelle F., Elkaim E., Stock N. *Inorg. Chem*. **2010**, *49*, 9852–9862. DOI: 10.1021/ic101128w.
55. Benecke J., Grape E.S., Fuß A., Wöhlbrandt S., Engesser T.A., Inge A.K., Stock N., Reinsch H. *Inorg. Chem*. **2020**, *59*, 9969–9978. DOI: 10.1021/acs.inorgchem.0c01124.
56. Tranchemontagne D.J., Hunt J.R., Yaghi O.M. *Tetrahedron* **2008**, *64*, 8553–8557. DOI: 10.1016/j.tet.2008.06.036.
57. Zhong H., Ly K. H., Wang M., Krupskaya Y., Han X., Zhang J., Zhang J., Kataev V., Büchner B., Weidinger I.M., Kaskel S., Liu P., Chen M., Dong R., Feng X. *Angew. Chem. Int. Ed.* **2019**, *58*, 10677–10682. DOI: 10.1002/anie.201907002.
58. Jia H., Yao Y., Zhao J., Gao Y., Luo Z., Du P. *J. Mater. Chem. A* **2018**, *6*, 1188–1195. DOI: 10.1039/C7TA07978H.
59. Yu B., Geng S., Wang H., Zhou W., Zhang Z., Chen B., Jiang J. *Angew. Chem.* **2021**, *133*, 26146–26152. DOI: 10.1002/ange.202110057.
60. Volkringer C., Loiseau T., Guillou N., Férey G., Elkaïm E., Vimont A. *Dalton Trans.* **2009**, *12*, 2241–2249. DOI: 10.1039/B817563B.
61. Steenhaut T., Filinchuk Y., Hermans S. *J. Mater. Chem. A* **2021**, *9*, 21483–21509. DOI: 10.1039/D1TA04444C.
62. Hwang Y.S., Liu J., Lenhart J.J., Hadad C.M. *J. Colloid Interface Sci.* **2007**, *307*, 124–134. DOI: 10.1016/j.jcis.2006.11.020.

Received 10.05.2024
Accepted 06.07.2024